ISSN 1751-8822

Evaluation of the front-fixing method capabilities for numerical modelling of field diffusion in high-temperature superconducting tapes

I.O. Golosnoy   J.K. Sykulski

Electrical Power Engineering Research Group, School of Electronics and Computer Science, University of Southampton, Highfield, Southampton SO17 1BJ, UK
E-mail: ig@ecs.soton.ac.uk

Abstract: Application of a finite-volume front-fixing method for modelling the electric field and associated power loss in high-temperature superconductors − or other similar strongly nonlinear phenomena − is considered. Advantages of the scheme are discussed and implementation challenges highlighted. Particular attention is paid to conservation properties of the algorithm and accurate solutions close to the transition boundaries. The algorithm is tested using an analytical solution for a plane superconducting tape problem with a transport current and a moving front.

1 Introduction

Diffusion equations are widely used to describe various electromagnetic processes. Formulations of field variations in terms of diffusion allow to utilise many numerical methods developed previously for heat and mass transport [1]. But often the modelling of the diffusion equation encounters problems with strong nonlinearity because of extreme variations in material properties with field changes, for example, as encountered in high-temperature super-conductivity [2], or with magnetic phase transitions because of Joule heating [3].

It was suggested to model AC losses in high-temperature superconducting (HTS) tapes as a diffusion process [2, 4]. Extreme variations in material properties with the field result in computational complications when conventional techniques are used because of extreme nonlinearity. For example, an explicit scheme requires small time steps [4]. For a multi-dimensional case, the mesh structure is also affected by stability criteria [2]. Rhyner [5] found that front-type solutions do exist in the system. This was confirmed later by numerical simulations [2, 4]. Since field variation at the front is severe, an effective algorithm should take into account the front motion explicitly.

This paper deals with modelling of field diffusion in an HTS tape with a moving front boundary. The motion is assumed to be a complex function of the solution itself. Many numerical methods developed previously, such as front tracking or re-meshing techniques, are often not able to cope with such a strong coupling [6]. On the other hand, the transformations proposed by Landau (see [6] for details) introduce a co-ordinate system in which all of the spatial boundaries are fixed. Under the transformation, the new computational domains remain the same with an additional nonlinear equation for the boundary motion. This allows keeping nodes close to the interface independent of the motion, which gives higher accuracy for the same number of nodes used. Inevitably, there is a price for such an improvement: the conservation laws in the new system must be modelled carefully and iterations are required to resolve nonlinear coupling between field diffusion and the interface displacement. The main challenges are the implementation of conservation laws at the moving boundaries and an effective mesh refinement. These issues are addressed here. The solution quality is assessed using a simplified system with a known analytical solution.

2 Formulation of the problem

2.1 Governing equations, tape geometry and material properties

It is possible to formulate the problem in terms of both magnetic or electric field diffusion [4, 5]. The electric field

418

IET Sci. Meas. Technol., 2008, Vol. 2, No. 6, pp. 418−426
doi: 10.1049/iet-smt:20080085

formulation is preferable for HTS materials with nonlinear properties since it provides much more stable solutions [2, 4]. For this case, the governing equation takes the form

$$\text{curl}(\text{curl}\,\boldsymbol{E}) = -\mu_0 \frac{\partial \boldsymbol{J}}{\partial t} \qquad (1)$$

with electric field $\boldsymbol{E}$, current density $\boldsymbol{J}$ and magnetic permeability of vacuum μ_0.

Normally, the width a of HTS ceramic tapes is much greater than its thickness $2b$ (Fig. 1) and for the tapes much longer than $2b$ (1) can be written for single components of the electric $\boldsymbol{E}$ and magnetic $\boldsymbol{H}$ fields with all quantities dependent on the z coordinate only. The boundary condition at the centre of the tape exploits the symmetry of the problem

$$\left.\frac{\partial E_y}{\partial z}\right|_{z=b} = 0 \qquad (2)$$

whereas the electric field at the tape surface is controlled by Faraday's and Ampere's laws. For example, consider an HTS tape carrying a transport current $I(t)$ with density $J_0(t) = (2ab)^{-1}I(t)$. For the z-axis looking inside the tape $bJ_0 = -H_x(z=0)$ and

$$-\left.\frac{\partial E_y}{\partial z}\right|_{z=0} = -\mu_0 \left.\frac{\partial H_x}{\partial t}\right|_{z=0} = \mu_0 b \frac{\partial (J_0)_y}{\partial t} \qquad (3)$$
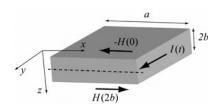
For simplicity, the coordinate indices in E and J are omitted for the rest of the paper.

HTS materials exhibit the flux creep $E-J$ characteristic. This is often described by Rhyner's power law [5]

$$\frac{E}{E_c} = \left(\frac{J}{J_c}\right)^{\alpha} \qquad (4)$$

where the critical current density $J_c \simeq 10^9\,\text{A m}^{-2}$ corresponds to a critical electric field $E_c \simeq 10^{-4}\,\text{V m}^{-1}$ and a large power exponent α which could be about 20. Substitution of (4) into (1) finally results in a formulation of the problem in terms of the electric field only [2]. It is convenient to introduce dimensionless variables.

θ for time: $t = \theta \cdot \mu_0 J_c E_c^{-1} b^2$,

Figure 1 *Geometry of a rectangular HTS tape carrying a transport current I(t)*

ξ for space: $z = \xi \cdot b$,

e for electric field: $e = E \cdot E_c^{-1}$,

i for current density: $i = J \cdot J_c^{-1}$,

and to rewrite (1)–(4) as follows

$$\frac{\partial}{\partial \theta}\left(\text{sign}e \cdot |e|^{1/\alpha}\right) = \frac{\partial^2 e}{\partial \xi^2} \qquad (5)$$

$$\left.\frac{\partial e}{\partial \xi}\right|_{\xi=0} = -\frac{\partial i_0}{\partial \theta} \qquad (6)$$

$$\left.\frac{\partial e}{\partial \xi}\right|_{\xi=1} = 0 \qquad (7)$$

$$e = i^{\alpha} \qquad (8)$$

2.2 Conservation laws

The problems (5)–(8) have purely Neumann boundary conditions and integration of (5) over the time and space domains results in a conservation integral

$$\int_0^1 \text{sign}e \cdot |e|^{1/\alpha}\mathrm{d}\xi = i_0(\theta) - i_0(0) \qquad (9)$$

2.3 Analytical solution

For front propagation problems, it is common [7] to search a solution which depends on a single variable

$$e(\theta, \xi) = e(w\theta - \xi) \equiv e(r), \quad r = w\theta - \xi \qquad (10)$$

and describes a propagation of the field into the material with constant velocity w. Substitution of (10) into (5) provides an ordinary differential equation over r. The latter has a solution only for specific boundary conditions, namely

$$i_0(\theta) = w^{1/(\alpha-1)}\left(\frac{\alpha-1}{\alpha}w\theta\right)^{\alpha/(\alpha-1)}, \left.\frac{\partial e}{\partial \xi}\right|_{\xi=0}$$
$$= -w^{\alpha/(\alpha-1)}\left(\frac{\alpha-1}{\alpha}w\theta\right)^{1/(\alpha-1)}, \quad 0 \le \theta \le 1/w \qquad (11)$$

In this case, the field evolution is given by

$$e(\theta, \xi) = \left(\frac{\alpha-1}{\alpha}w(w\theta - \xi)\right)^{\alpha/(\alpha-1)}, \quad \text{for } (w\theta - \xi) > 0$$

$$e(\theta, \xi) \equiv 0, \quad \text{for } (w\theta - \xi) \le 0 \qquad (12)$$

The solution (12) exists only during a limited time interval $0 \le \theta \le 1/w$ and, of course, it satisfies the conservation integral (9). The result (12) is similar to those obtained in [5] for the case of an external magnetic field. Equation (12)

is used in the paper to test the performance of different numerical techniques for the solution of the problems (5)–(8).

3 Numerical techniques

3.1 Fixed grid

Second-order approximations in both space and time require a semi-implicit approximation for (5) [1], but the often severe restrictions because of its poor monotonic properties force the selection of fully implicit methods. For this reason, a parametric family of numerical schemes is considered here with an implicit parameter p. [A semi-implicit method with $p = 0.5$ is used in the paper for predictions because diffusion fluxes are limited for the test problems (11) and (12).] Integrals of (5) around each node m over one time step provide a set of conservative equations in the bulk material [8], which are represented on a fixed grid by (13), where a subscript notation to denote discretisations of space (e.g. ξ_m) is used and superscripts (e.g. θ^n) indicate time

$$
((Ce)_m^{n+1} - (Ce)_m^n)0.5(\xi_{m+1} - \xi_{m-1})
$$
$$
= (\theta^{n+1} - \theta^n)\left(\frac{e_{m+1}^{n+p} - e_m^{n+p}}{\xi_{m+1} - \xi_m} - \frac{e_m^{n+p} - e_{m-1}^{n+p}}{\xi_m - \xi_{m-1}}\right) \quad (13)
$$

with specific capacity $C = |e|^{1/\alpha - 1}$, if $e > 0$ and $C = 0$ for zero field. The boundary condition (6) is approximated by integration of the input flux at $\xi = 0$ resulting in

$$
((Ce)_0^{n+1} - (Ce)_0^n)0.5(\xi_1 - \xi_0)
$$
$$
= (\theta^{n+1} - \theta^n)\left(\frac{e_1^{n+p} - e_0^{n+p}}{\xi_1 - \xi_0}\right) + i_0(\theta^{n+1}) - i_0(\theta^n) \quad (14)
$$

The approximation for the symmetry condition (7) is similar. The linearisation is introduced in (13) in order to implement an effective iteration algorithm. The capacities C are established from the previous iteration, which make the systems (13) and (14) linear and it can therefore be inverted effectively via a tridiagonal algorithm [1]. Because of the conservation condition (9), the systems (13) and (14) are parabolic at least at part of the computational domain and the inversion algorithm is stable.

Equation (13) highlights the two main complications in describing high-temperature superconductors. In many cases, the field penetrates the material to a depth which varies a lot with time, responding to the transport current changes. This forces the placement of the grid points through the whole thickness of the tape. Moreover, the problem (5) is very nonlinear for $\alpha \simeq 10$ (and above, which are typical values) and the distance between nodes should be relatively small to accommodate instances of shallow penetration. This is especially important when the tape

operates at current densities close to the critical value as released Joule heat could change the properties of the superconductor significantly [9]. The second problem is directly linked to the conservation law (9). If (13) and (14) are solved by an explicit ($p = 0$) scheme [4], the property (9) strictly holds true. But stability criteria are severe for such an explicit scheme and its use in parametric studies could be restricted by computational time constrains. Although implicit schemes are unconditionally stable, their usage also has some drawbacks. Since (13) is nonlinear, it has to be solved iteratively. This means that the discrete approximation for the conservation law (9) is not strictly valid any more at intermediate iteration steps. Conditions to end iterations are directly linked to (9) and they are severe, especially for a large exponent α. It has been found that for high-quality results at $\alpha = 9$ the maximum discrepancy between the final iterations should be smaller than 10^{-18} in L_1 norm.

3.2 Adaptive meshes

Adaptive meshes allow to dynamically arrange nodes in the volumes penetrated by the field. Ideally, this would significantly decrease the number of nodes required, but is only effective for problems with weak nonlinearity. In our case, a simple interpolation of the electric field into new adapted positions results in breaking the conservation law (9). Careful interpolation is possible but it is accompanied by mathematical complications.

Thus the objective is for a numerical technique to adapt the nodes' positions automatically and, as a result, satisfy conservation laws easily.

3.3 Front-fixing method

The Landau transformation (Fig. 2) utilises new positional variables (one for each domain). In the plane case, an introduction of $u = (\xi - s_1(\theta))/(s_2(\theta) - s_1(\theta))$ fixes the extent of the region with edges $s_1(\theta)$ and $s_2(\theta)$ to the domain $0 \le u \le 1$ [6]. For the test front problems (11) and (12), only one domain with a boundary at $s_1 = 0$ and $s_2 = s$ (where the field has disappeared) needs to be considered, constituting an additional simplification. Using the results from [10], the conservation form [8] of (5) for u may be written as

$$
\frac{\partial}{\partial \theta}\left(s \cdot \mathrm{sign}e \cdot |e|^{1/\alpha}\right) = \frac{\mathrm{d}s}{\mathrm{d}\theta}\frac{\partial}{\partial u}\left(u \cdot \mathrm{sign}e \cdot |e|^{1/\alpha}\right) + \frac{1}{s}\frac{\partial^2 e}{\partial u^2}
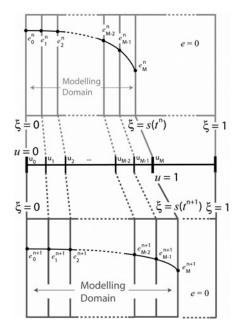$$
$$(15)$$

$$
\left.\frac{\partial e}{\partial u}\right|_{u=0} = -s\frac{\partial i_0}{\partial \theta} \quad (16)
$$

$$
e|_{u=1} = 0 \quad (17)
$$

Figure 2 *Landau transformation introduces new positional variables for which the fixed interval [0,1] corresponds to a new coordinate system u*

Positions in real space ξ automatically adjust to accommodate the motion of the interface

with the conservation integral

$$s \int_0^1 \text{sign} e \cdot |e|^{1/\alpha} \mathrm{d}u = i_0(\theta) - i_0(0) \tag{18}$$

It should be noted that the combination of conditions (15)–(18) imposes an additional limitation on the field derivative at the front point $u = 1$

$$\left. \frac{\partial e}{\partial u} \right|_{u=1} = 0 \tag{19}$$

so that the condition (7) is satisfied at the domain boundary s and beyond it up to the symmetry line.

The Landau transformation introduces a co-ordinate system in which all of the spatial boundaries are fixed to 0 or 1. Under the transformation, the new computational domain remains the same with an additional advection term in (15) and nonlinear equations for the boundary motion (18). This allows treating the nodes close to the interface as being independent of the motion, which gives higher accuracy for the same number of nodes used. The conservation form of (15)–(18) ensures that there are no artificial current sources [10].

Equations (15)–(18) represent a typical Stefan problem with the so-called implicit moving boundary [6] and strongly nonlinear specific capacity. The interface position is not strictly defined in this case and the displacement s is

selected by physical considerations. The transformation point is assumed to be one with zero value of both the electric field and its first derivative.

3.4 Numerical scheme

In order to derive a finite-volume scheme, space is discretised at $M+1$ points. The points are defined by a fixed discretisation of u and they are written as $u_0 = 0$, u_1, ..., $u_M = 1$. The finite-volume discretisation [8] of (15)–(17) is based on integration around the nodes and is fairly straightforward [10], for example, for the node m

$$\left(s^{n+1}(Ce)_m^{n+1} - s^n(Ce)_m^n \right) 0.5\left(u_{m+1} - u_{m-1} \right)$$
$$= \left(s^{n+1} - s^n \right)\left(u_{m+0.5}(Ce)_{m+0.5}^{n+p} - u_{m-0.5}(Ce)_{m-0.5}^{n+p} \right)$$
$$+ \frac{(\theta^{n+1} - \theta^n)}{s^{n+p}} \left(\frac{e_{m+1}^{n+p} - e_m^{n+p}}{u_{m+1} - u_m} - \frac{e_m^{n+p} - e_{m-1}^{n+p}}{u_m - u_{m-1}} \right) \tag{20}$$

with specific capacity $C = |e|^{1/\alpha - 1}$, if $e > 0$ and $C = 0$ for zero field. An approximation for an intermediate point is given by linear interpolation: $e_{m+0.5} = 0.5(e_m + e_{m+1})$. The boundary equations are approximated in a consistent way to conserve current [10], for example, for (16)

$$\left(s^{n+1}(Ce)_0^{n+1} - s^n(Ce)_0^n \right) 0.5\left(u_1 - u_0 \right)$$
$$= \left(s^{n+1} - s^n \right)\left(u_{0.5}(Ce)_{0.5}^{n+p} \right)$$
$$+ \frac{(\theta^{n+1} - \theta^n)}{s^{n+p}} \left(\frac{e_1^{n+p} - e_0^{n+p}}{u_1 - u_0} \right) + i_0(\theta^{n+1}) - i_0(\theta^n) \tag{21}$$

The approximation for (17) is straightforward and omitted here. The interface position s^{n+1} is defined implicitly by requiring that

$$s^{n+1} \sum_{m=0}^{M-1} 0.5\left((Ce)_{m+1}^{n+1} + (Ce)_m^{n+1} \right)\left(u_{m+1} - u_m \right)$$
$$= i_0(\theta^{n+1}) - i_0(0) \tag{22}$$

3.5 Implementation

The set of simultaneous equations (20)–(22) involves the unknown future electric field together with the future interface position. Since all of the equations are coupled, the entire system must be solved simultaneously in order to conserve current. This is potentially very demanding in terms of computing times. It is suggested to introduce two enclosed iteration cycles to solve the system effectively. At an internal cycle, the value of the interface position s^{n+1} is fixed. The specific capacity C^{n+1} is taken from the previous iteration and (20)–(21) become linear so that they can be quickly inverted by a tridiagonal algorithm. When consistent solution of (20) and (21) is reached for a fixed s^{n+1} (with the maximum discrepancy between the final iterations smaller than 10^{-10} in L_1 norm), the interface

position is updated via (22) until $\left|1 - s_{(k)}^{n+1}/s_{(k+1)}^{n+1}\right| \geq 10^{-3}$. It has been found that the algorithm requires a significantly smaller number of iterations to reach a consistent solution in comparison with those on a fixed grid.

The transformed equation (20) includes an advection term on the right-hand side. The effective velocity is proportional to the interface displacement and capacity C. Since $C \simeq |e|^{-1}$ and it is large close to the interface $u = 1$, where $e \ll 1$, the modelling indeed faces problems with oscillations at the front. Such non-monotonic behaviour could be avoided by using up/down-wind approximation for the advection term [1, 10], but it decreases the order of space approximation. On the other hand, a reversible flux transport corrected algorithm [11] provides reasonable second-order accuracy in space and time with only $\sim$25% increase in computational cost. A slight modification of the method [11] was used in the paper to allow better modelling of high velocity cases. An additional improvement can be achieved by applying a variety of total variation diminishing methods [12].

3.6 Mesh generation

It is preferable to place grid nodes close to the interface to model the front displacement with higher accuracy. On the other hand, switching to non-uniform grid decreases the space approximation in diffusion equation (20) from second order to first order. The best way to avoid complications is to condense the nodes gradually. The following algorithm was implemented: $u_0 = 0$, $u_{m+1} = u_m + q^m h$, $m = \overline{0, M-1}$, with multiple $0.8 \leq q \leq 1$ and initial step $h = u_1 - u_0$ as defined by the domain size

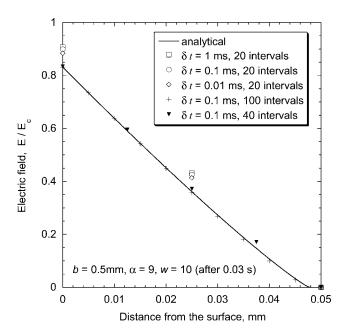$$1 = \sum_{m=0}^{M-1} \left(u_{m+1} - u_m\right) = h\left(\frac{1-q^M}{1-q}\right) \qquad (23)$$

The particular choice in (23) ensures that the grid nodes are adjusted to the front location $u = 1$.

4 Results

For test purposes, the HTS tape $2b = 1$ mm thick was studied. The transport current was selected from (11) to provide the dimensionless front velocity $w = 10$. Full penetration takes place after $t \simeq 0.3142$ s, but the paper is focused on the initial stages of the process keeping in mind cycling field penetration under AC current load. The ways in which particular choices of the time step and the number of nodes affect the accuracy of predictions were analysed in some detail. Most comparisons were conducted with the exponent $\alpha = 9$, but the performance using other values of α was also investigated.

4.1 Fixed grid

Decreasing the time step improves the accuracy of the model only a little (Fig. 3), indicating that the major errors are

Figure 3 *Exact solution is available for specific initial and boundary conditions (11)*

The electric field inside the HTS tape after $t = 0.03$ s is predicted on fixed grids and compared with the analytical solution

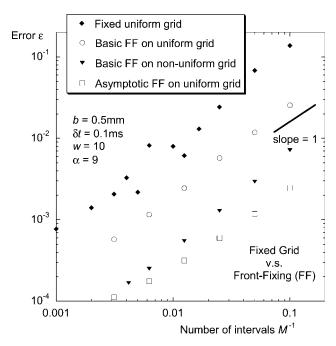The accuracy of the model is affected more by the space discretisation rather than the time step

dominated by the coarse discretisation of space. Placing a reasonable number of grid points ($\sim$10) over the penetration depth significantly improves the predictions. The details showing the variation of errors with an increasing number of space intervals M are plotted in Fig. 4. The error ε is taken in a continuous norm

$$\varepsilon = \max_{m=0}^{M}\left|e_m^{\text{analytical}} - e_m^{\text{model}}\right|$$

A slope of the $M^{-1} - \varepsilon$ curve in log–log coordinates indicates only the first-order space approximation. This is a slightly surprising result since a second-order approximation is used for the discretisation of (13) and (14). The reason for this behaviour can be explained by summing the right- and left-hand sides of (13) over the grid nodes and time intervals. Together with (14), the sum provides a finite-volume approximation for the conservation integral (9). Consequently, (9) is approximated using a trapezoidal rule which has only $O(M^{-1})$ accuracy because of a singularity of the first derivative of the integrated function

$$e^{1/\alpha} \sim (w\theta - \xi)^{1/(\alpha-1)}$$

at the front $\xi \to w\theta$. Another observation is a strong noise in the errors. This can be attributed to the fact that even for a large number of points, the nodes are 'switched on' in a stepwise manner: the position of interface with $e = 0$ jumps from node to node at a particular time.
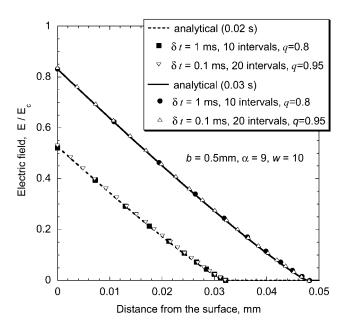
422

© The Institution of Engineering and Technology 2008

IET Sci. Meas. Technol., 2008, Vol. 2, No. 6, pp. 418–426

doi: 10.1049/iet-smt:20080085

Figure 4 *Errors in predictions of an electric field inside the HTS tape after $t = 0.03$ s reveal an approximately $O(M^{-1})$ accuracy for both fixed grid method and front-fixing technique. (The errors are estimated in continuous C norm.)*

The accuracy of the fixed grid method is significantly lower in comparison even with the basic front-fixing method

It is interesting to note that the number of iterations at each time step is almost independent of the space step. It slowly decreases with the time step decreasing and stays around 230−250 for $\delta t \simeq 1$ ms. This number looks surprisingly high, but is a direct consequence of the strongly nonlinear capacity C. It is very difficult to satisfy the conservation integral (9) using the simple iteration procedure implemented in the study. Newton's method could improve the convergence rate, but its implementation is complicated because of the zero field and field derivative in a significant part of the computational domain [4].

4.2 Front-fixing method: general observations

Predictions from the method are summarised in Figs. 5 and 6. Even for a small total number of points, the accuracy is high and gradually increases with increasing number of nodes. Field penetration is controlled by field diffusion at the interface. The front-fixing method follows the interface (Fig. 6) and there are always nodes close to the penetration point (Fig. 5). As a consequence, the accuracy of the front-fixing method is excellent.
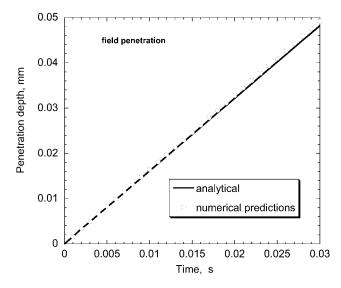
It has been found that for a small number of nodes, it is computationally profitable to gather them towards the interface s. For a large M, more uniform grids are preferable. (For example, for $q = 0.8$, $M = 11$ and the last interval is approximately one-tenth of the first one, whereas for $q = 0.95$, $M = 21$ and the ratio is one-third only.) This is

Figure 5 *Front-fixing method predictions of electric field inside the HTS tape with $\alpha = 9$ after $t = 0.02$ s and $t = 0.03$ s*

The nodes are gathered towards the interface to provide better approximation of the field penetration

The method is less sensitive to variations of the time step and number of nodes in comparison of the fixed grids

Figure 6 *Interface position is predicted to vary linearly with time*

Numerical results of the front-fixing are in excellent agreement with the analytical solution for $\alpha = 9$, $w = 10$, $b = 0.5$ mm

due to the fact that for small M the errors are dominated by poor approximation of the interface s, whereas for larger M the main source of errors is a non-uniformity of the grid.

Similarly to the fixed grid case, the number of iterations in the internal loop (for the fixed future interface position $s_{(k+1)}^{n+1}$) at each time step is almost independent of the space steps. It decreases slowly with decreasing time step and stays around

Table 1 Effect of an initial guess of the interface position on the number of necessary iterations

Parameter β	Total number of iterations per time step	Number of external iteration cycles over $s_{(k)}^{n+1}$
0.1	250−340	3
0.25	250−340	3
0.5	250−330	3
0.75	230−320	3
0.9	160−220	2
1.0	90−120	1
1.1	350−450	3−4
1.25	350−570	3−5
1.5	600−850	5−7
2.0	610−1030	5−8

100−120 per each external cycle for $\delta t \simeq 1$ ms. This number is two times smaller in comparison with the fixed grid technique. This should be expected since the conservation integral (9) is approximately satisfied in the front-fixing method by an appropriate choice of the interface position $s_{(k+1)}^{n+1}$ at each iteration via (22) in the external iteration cycle implemented in the study.

The effect of an initial estimation $s_{(0)}^{n+1}$ of the interface on the number of iterations has also been studied. The following parametric variations in $s_{(0)}^{n+1}$ were introduced

$$s_{(0)}^{n+1} = s^n + \beta \cdot \delta s^n = s^n + \beta\left(s^n - s^{n-1}\right) \qquad (24)$$

with the parameter $\beta \in [0.1, 2.0]$. The analytical solution suggests that $\beta = 1$ would be an optimal choice since the interface velocity is constant for the test problem. This is confirmed by the simulations with the results summarised in Table 1. Generally, the closer the initial estimation to the real position, the quicker a consistent solution is reached. But the dependence is not linear; it is much more profitable to underestimate the interface displacements ($\beta < 1$), in which case the convergence is achieved after only three external cycles, even for $\beta = 0.1$.
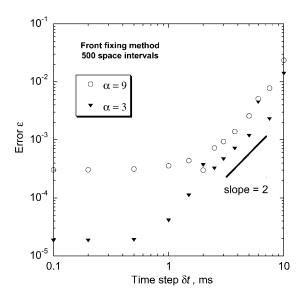
One drawback of the method is an additional artificial diffusion introduced into the system by the discretisation of the advection term. As a result, the interface position is slightly overestimated when compared with what the analytical model suggests.

4.3 Front fixing method: error analysis

Errors resulting from time discretisation were studied by varying δt between 0.1 and 10 ms for a large number of space intervals

$M = 500$. A semi-implicit approach with $p = 0.5$ provides a second-order approximation in time $O(\delta t^2)$ (Fig. 7). This conclusion is valid for both cases of weak ($\alpha = 3$) and strong ($\alpha = 9$) nonlinearities. It can be seen that the errors saturate at $\delta t \simeq 1$ ms which indicates predominance of space residuals. Indeed, a slope of $\log-\log M^{-1} - \varepsilon$ curve (Fig. 4) suggests only the first-order $O(M^{-1})$ for the spatial accuracy. Again, this can be explained by the singularity of the solution at the front. The front fixing strictly satisfies the conservation law (18) by adjusting the interface position s through (22). Since a trapezoidal rule is used in (22), s is estimated with $O(M^{-1})$ accuracy. The situation can be improved by noting that the main errors appear at the front $\xi \rightarrow w\theta$. A non-uniform mesh (23) could be gradually condensed towards the boundary balancing gains in an accurate calculation of (22) and losses because of non-uniform grid for diffusion equation (20). The case $q(2M) = \sqrt{q(M)}$ with $q(M = 10) = 0.8$ is presented in Fig. 4, improving the accuracy by a factor of 4, although it is still the case that $\varepsilon \simeq O(M^{-1})$.
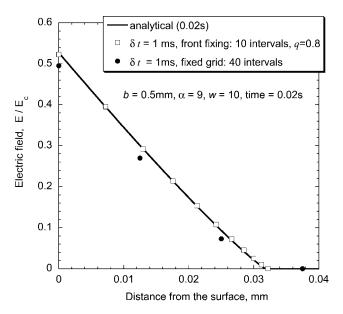
For the test case (12), an asymptotic at the front is known. Therefore higher accuracy can be achieved in the numerical integral (22) by replacing the trapezoidal rule for at last two nodes by an exact solution. This has proved to be very effective for a small number of M, when the main error is indeed due to the last two nodes. As M increases, the error starts to fill further nodes adjusted to the boundary and the non-uniform grid provides a competitive solution. The latter is actually preferable because it does not rely on the known properties of the solution and can be applied for any currents, not just the specific one (11) used in the test.

Figure 7 *Effect of the time step δt on the predictions of an electric field*

The results are for $t = 0.03$ s and dimensionless velocity $w = 10$
The results indicate that the algorithm has at least a second-order accuracy in time
Because of lower spacial accuracy, an effect of a saturation of the errors with $\delta t \rightarrow 0$ is observed at $\delta t \simeq 1$ ms for quite large values of $M = 500$
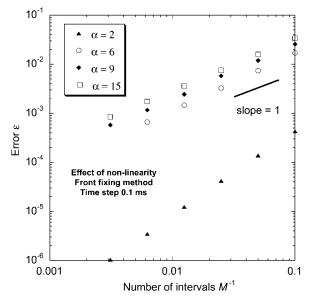
Figure 8 *Predicted variation of the electric field inside the HTS tape*

The numerical predictions of the front-fixing and fixed grid techniques are compared with an analytical solution at $t = 0.02$ s The front-fixing method places the nodes at the important locations and requires significantly fewer discretisation points to obtain a similar accuracy

4.4 Comparative study

The study of the electric field penetration into HTS tapes suggests that the same accuracy could be achieved from the front-fixing method using four times fewer grid points (Fig. 8) than needed for the fixed grid. The analysis of the errors (Fig. 4) suggests that this conclusion is valid (approximately) for any number of nodes M. Moreover,

Figure 9 *Errors of the front-fixing method for different exponents α*

Predictions at $t = 0.03$ s suggest $O(M^{-1})$ accuracy for large α

each time increment in the front-fixing method usually requires a similar number of iterations in comparison with the fixed grid technique (Table 1), although the presence of the advection term increases the computational complexity by a quarter. The average overall reduction in computational effort is about four times in the case of the test problem, which is significant.

The effect of the exponent α on accuracy of the front-fixing method is demonstrated in Fig. 9. Errors quickly decay $O(M^{-1.75})$ for a weak nonlinearity $\alpha = 2$ and the method exhibits an extremely efficient performance. In a highly nonlinear regime, $\alpha \simeq 10$, the errors are significantly higher and the accuracy order is lower $O(M^{-1})$. Nevertheless, errors stay at approximately the same level when increasing α from 6 to 15 suggesting that the front-fixing technique could be effectively applied to extremely nonlinear processes.

5 Conclusions

The use of a front-fixing method for modelling highly nonlinear diffusion processes has been demonstrated using the case of electromagnetic field penetration into a high-temperature superconducting tape. The following conclusions can be drawn from this work.

(a) There are several advantages of using a front-fixing method for modelling of superconductivity phenomena, in particular, high accuracy can be obtained with a small number of grid points and large time increments.

(b) Potential problems with implementation of conservation laws and complex boundary conditions have been considered and various remedies suggested.

(c) Standard numerical methods for advection problems with diffusion can be utilised.

(d) It has been shown that the interface motion can be predicted on a coarse irregular mesh since the interface position is fixed in new coordinates.

6 References

[1] TANNEHILL J.C., ANDERSON D.A., PLETCHER R.H.: 'Computational fluid mechanics and heat transfer' (Taylor & Francis, Washington, London, 1997, 2nd edn.)

[2] SYKULSKI J.K., ROTARU M., STOLL R.L.: '2D modeling of field diffusion and AC losses in high temperature superconducting tapes', *IEEE Trans. Magn.*, 2000, **36**, (4), pp. 1178–1182

[3] KUDASOV Y.B.: 'Magnetic field diffusion during a metal–insulator phase transition', *Tech. Phys.*, 1998, **43**, (12), pp. 1440–1444

[4] SYKULSKI J.K., STOLL R.L., MAHDI A.E.: 'Modelling HTc superconductors for AC power loss estimation', *IEEE Trans. Magn.*, 1997, **33**, (2), pp. 1568–1571

[5] RHYNER J.: 'Magnetic properties and AC-losses of superconductors with power law current–voltage characteristics', *Physica C*, 1993, **212**, pp. 292–300

[6] CRANK J.: 'Free and moving boundary problems' (Clarendon Press, Oxford, 1984)

[7] VINOKUR V.M., FEIGELMAN M.V., GESHKENBEIN V.B.: 'Exact solution for flux creep with logarithmic U(J) dependence – self-organized critical state in high-Tc superconductors', *Phys. Rev. Lett.*, 1991, **67**, (7), pp. 915–918

[8] LEVEQUE R.J.: 'Finite volume methods for hyperbolic problems' (Cambridge University Press, Cambridge, 2002)

[9] BERGER K., LEVEQUE J., NETTER D., DOUINE B., REZZOUG A.: 'AC transport losses calculation in a Bi-2223 current lead using thermal coupling with an analytical formula', *IEEE Trans. Appl. Supercond.*, 2005, **15**, (2), pp. 1508–1511

[10] ILLINGWORTH T.C., GOLOSNOY I.O.: 'Numerical solutions of diffusion-controlled moving boundary problems which conserve solute', *J. Comput. Phys.*, 2005, **209**, (1), pp. 207–225

[11] BORIS J.P., BOOK D.L.: 'Flux-corrected transport. III: Minimal-error FCT algorithms', *J. Comput. Phys.*, 1976, **20**, pp. 397–431

[12] TORO E.F.: 'Riemann solvers and numerical methods for fluid dynamics: a practical introduction' (Springer, Berlin, 1999, 2nd edn.)